Heliyon 7 (2021) e07947

Contents lists available at ScienceDirect

Heliyon

journal homepage: www.cell.com/heliyon

Research article

Energy, exergy, and environmental assessment of a small-scale solar organic Rankine cycle using different organic fluids

Geanette Polanco Piñerez [a], Guillermo Valencia Ochoa [b,*], Jorge Duarte-Forero [b]

[a] UiT, The Arctic University of Norway, Industrial Department, Campus Narvik, Norway
[b] Universidad del Atlántico. Departamento de Ingeniería Mecánica, Carrera 30 Número 8 - 49, Puerto Colombia, Área Metropolitana de Barranquilla, Colombia

ARTICLE INFO

Keywords:
3E
Organic rankine cycle
Global solar radiation
Exergy analysis
Life cycle assessment

ABSTRACT

This article presents an energetic, exergetic, and environmental (3E) analysis of a solar powered simple Rankine Organic Cycle (ORC). The ORC is simulated using three organic working fluids, such as Toluene, Cyclohexane, and Acetone, meanwhile the solar system uses thermal oil Therminol 75. The present study shows the performance of this coupled system using historical solar annual radiation data from four of the highest solar potential locations in Colombia. Data used correspond to data for the cities Rancho Grande, Puerto Bolivar, Manaure, and Nazareth. Simulations were performed using commercial programs as MATLAB® and REFPROP 9.0. Energy production, the energy and exergetic efficiencies of the system, the exergy destruction was calculated based on the input of the global solar radiation. Effects generated by each working fluid in the solar powered ORC system was determined. It was stablished that the heat obtained in the solar collector in combination with a storage tank is incorporated during non-radiation hours guarantees the thermal stability of the working fluid in the ORC. The best performance corresponds to the Rancho Grande city, being the Toluene the corresponding working fluid with the highest energy (14.6%) and exergetic (7.37%) efficiencies, as well as the maximum power generation (5.50 kW) for October month, meanwhile, the highest exergy destruction values correspond in April. A sensitivity analysis of the individual elements of the system was performed. This study revealed the preference of a lower evaporator pinch point temperature, higher turbine thermal efficiency, pump thermal efficiency, and pressure ratio to obtain better energy and exergy efficiency of the solar powered ORC system. Additionally, the potential environmental impact of the system was evaluated through a Life Cycle Analysis, obtaining for the solar system solar collector has the highest environmental impact with 78557850 mPts. Meanwhile for the ORC, the turbine registers the most significant environmental impact with 295516 mPts (7.34%), when Toluene is used as a working fluid and copper as a construction material in the location of Rancho Grande. In conclusion, the potentiality of planning the operation of solar powered ORC was successfully evaluated for four specific locations in Colombia.

1. Introduction

The growing demand for energy worldwide due to the increase in the human population and the generation of more industries has led to a global concern to seek alternatives to meet this demand and at the same time reduce greenhouse gas emissions from conventional methods of energy generation [1]. According to the report provided by Jackson et al. [2]. The generation of energy, heat, and electricity dominate with 45% of global CO_2 emissions until 2017, followed by the emissions from industrial activities with 23%. It is estimated that in 2050 emissions will reach an increment of approximately 1.5–3 times [3]. Thus, alternative sources of energy generation, and efficient systems of energy conversion, appear as solutions to meet the needs of energy demand and decrease greenhouse gases [4].

Solar energy is an excellent source of pollution-free energy that reduces pollutant emissions derived from fossil fuels [1]. Technological improvements towards the increment in efficiency and reduction of costs of solar systems make solar energy an important energy production alternative [5]. In 2016, nations agreed to reduce greenhouse gas (GHG) emissions by, among other measures, increasing renewable energy technologies use [6]. On average, 3.3 million tons of carbon dioxide can be reduced by increasing renewable energy capacity by 1 GW [7]. The

* Corresponding author.
E-mail address: guillermoevalencia@mail.uniatlantico.edu.co (G. Valencia Ochoa).

https://doi.org/10.1016/j.heliyon.2021.e07947
Received 2 May 2021; Received in revised form 21 July 2021; Accepted 3 September 2021

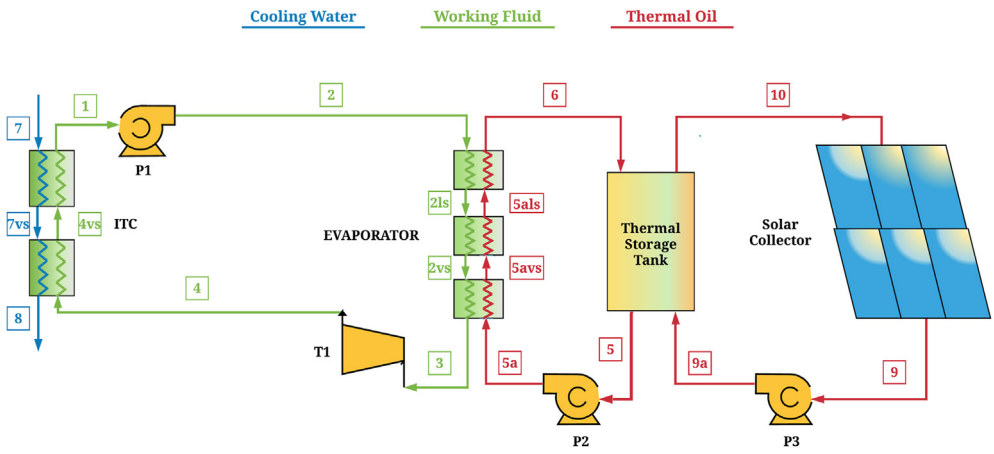

Figure 1. Schematic diagram of the solar-powered Organic Rankine Cycle system.

concentrated solar power (CSP) applications are appropriate for regions that receive high solar irradiation, such as the Department of Guajira in Colombia since they produce electricity or heat through an array of mirrors that originate a concentration of sunlight generating temperatures between 400 °C and 1000 °C at the concentration site.

An organic Rankine cycle (ORC), which is a Rankine cycle that, instead of using water as a working fluid, uses organic fluids to take advantage of medium and low-temperature heat sources to generate electricity in areas not connected to the national grid, as is the case in Guajira-Colombia. Due to its characteristics, the ORC is ideal for low scale power generation applications, up to approximately 50 MW comprising a good range of operating temperatures and working fluids [8], being more attractive to a conventional Rankine cycle due to higher efficiency in converting low-temperature heat into useful work since it uses organic fluids with low boiling temperatures [9, 10, 11]. Also, the performance and advantages of ORC have been investigated by experimental and simulation studies, including methodologies for the selection of the working fluid and optimization of parameters [12].

Thus, Sun et al. [13] evaluated the effect of operational parameters such as evaporation and condensation temperature and degree of superheat on the thermodynamic performance of an ORC system using low-temperature waste heat and R113 as working fluid. Feng et al. [14] made an experimental investigation of a 3 kW ORC fed by low-quality waste heat, and working fluid R245fa under different operating parameters. Pang et al. [15] experimentally compared an ORC system using binary mixtures of R245fa:R123 with different ratios to investigate the maximum net power with low heat temperature, setting temperatures of 383.15 K and 393.15 K. Feng et al. [16] experimentally analyzed the behavior of an ORC using R245fa, R123, and the mixtures of both working fluids. Li et al. [17] carried out experimental research of the performance of a small-scale ORC with R245fa as working fluid. Ashouri et al. [18] evaluated the thermodynamic performance of benzene, butane, pentane, isopentane, R123, and R245fa as working fluids of a Regenerative Organic Rankine Cycle (RORC) integrated with parabolic trough solar collector (PTCs). Tiwari et al. [19] conducted an energetic and exergetic analysis and multi-objective optimization of an ORC-solar system considering hexane/pentane, isohexane/pentane, and butane/-pentane mixtures.

The generation of electricity through the transformation of solar energy has taken place in the field of ORC, both in the study of small-scale and large-scale systems. Thus, Chacartegui et al. [20] and Casartelli et al. [21] studied power generation for 5MW plants, both with energy storage systems, the first using two indirect thermal energy storage models where the first design used Hitec XL as a heat transfer and storage fluid, and the second design with Therminol VPP-1 as a heat transfer fluid and Hitec XL for storage. Both authors concluded that Toluene is the best working fluid for their considerations with an efficiency of 31.5%. Cocco and Cau [22] carried out studies for a power generation capacity of 1 MW, comparing PTCs and Fresnel mirrors, concluding that PTCs are the best option, reaching an efficiency of 24%. On a smaller scale (20kW) Ferrara et al. [23] employed various solar-ORC arrays using PTC and different working fluids, achieving efficiencies of 20% with Acetone. Bellos & Tzivanidis [24] investigated an energetic and exegetic trigeneration-solar system driven by solar parabolic trough collector (PTCs) using six working fluids. The results revealed that toluene had the highest output efficiency in the base condition (27.97%). Wang et al. [25] studied the performance of an ORC system driven by solar parabolic collector (PCs) under transient conditions. Baccioli et al. [26] evaluated the energetic and exergy performance of three proposed configurations: Organic Rankine Cycle-compound parabolic concentrator solar (ORC-CPCs), Organic Rankine Cycle-evacuated tube collector solar (ORC-ETCs), and Organic Rankine Cycle-flate-plate collector solar (ORC-FPCs). Ashouri et al. [27] analyzed from an energetic and exergetic point of view a RORC driven flat-plate solar collector with storage tank using R245fa, R134a, pentane and toluene as working fluids. Similar work was performed by Ramos et al. [28] who maximized the electrical power considering the operational limits of the solar collector of two systems flat-plate solar collector (FPCs-ORC) and evacuated-tube collector-ORC (ETCs-ORC). Arteconi et al. [29] studied the influence of the electrical and thermal performance of an ORC system with evacuated tube solar collector and storage tank.

In Colombia, studies have been carried out to characterize solar potential in the northern region of Colombia [30], but this has not been applied to alternative energy generation systems that can operate in areas not connected to the electricity grid, such as ORC. Also, for this system in engine waste heat recovery applications for the Colombian industrial sector, Ochoa et al. [31] determined that the organic fluids toluene, Acetone, and cyclohexane presented good energetic and exergetic performances because they are dry and isentropic fluids with a high critical temperature, low global warming potential, and low ozone depletion potential.

On the other hand, one of the indicators that has acquired great relevance is the life cycle assessment (LCA) as a tool to determine the impact associated with the implementation of this type of technology. In this regard, Cioccolanti et al. [32] carried out a life cycle assessment of a small-scale solar organic Rankine cycle trigeneration system. The results showed that R245fa allows better environmental benefits compared to R245ca (140 μPt/kWh with R245fa and 160 μPt/kWh with R245ca). A similar study was conducted by Liu et al. [33] who presented a life cycle assessment of an organic Rankine cycle. The results showed that the construction phase contributed the most to the global warming potential (GWP).

Finally, the main contribution of this manuscript is to evaluate the potential for thermal power generation from non-conventional energy sources for areas with high solar potential in the Colombian Caribbean

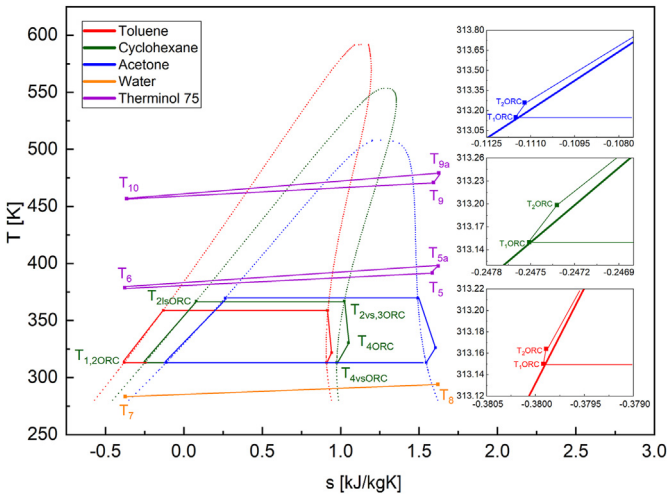

Figure 2. T-s diagram of organic fluids.

region, with emphasis on La Guajira. For this purpose, an energetic, exergetic, and environmental (3E) analysis of an Organic Rankine Cycle (ORC) driven by evacuated tube solar collector integrated with a thermal storage tank was conducted, considering three working fluids: Toluene, Cyclohexane, and Acetone. Thus, it is expected to contribute with information related to the environmental impacts associated with the implementation of this type of technology in off-grid areas, in addition to the performance in terms of energy and exergy, under real operating conditions.

2. Methodology

2.1. System description

Used Solar-ORC system configuration used in this work consists of two well-differentiated systems, a two stages solar heating circuit and an organic Rankine cycle, in addition to a cooling water supply. The solar circuit works with Therminol 75 as a thermal oil working fluid. In the first stage of the solar circuit, identified by the points 9–10, the fluid is driven by the pump P3 to the storage tank, which acts as a heat exchanger, where it discharges the heat and then passes to the solar collector where it receives heat from the solar radiation. A storage tank is used to provide continuous heat supply when solar radiation is insufficient. Then, in the second stage of the solar circuit, the fluid gains heat from the first stage at the thermal tank, and it passes to the evaporator drove by a pump (P2). The ORC identified for points 1–4 in Figure 1 is composed of a three-stage evaporator, a turbine (T1), a two-stage condenser (ITC), and a pump (P1). In the evaporator, the thermal oil transfers heat to the working fluid (Toluene, Cyclohexane, and Acetone), which increases its temperature as it passes through the three stages of the evaporator where it is preheated, evaporated, and finally reaches the superheated steam condition. Then the working fluid in a state of superheated steam enters the turbine (T1) at high pressure and generates work. The gaseous fluid exits the turbine at low pressure and temperature, and it goes to the condenser where it transfers heat to a low-temperature sump condensing to saturated liquid condition and then being driven by a pump (P1) which circulates it back to the evaporator, completing the cycle. The cooling water supply is identified by points 7–8.

The Temperature-entropy diagram of the thermodynamic cycles is presented in Figure 2 for Rancho Grande location using the three organic working fluids. In the three case studies presented, the solar collector useful heat gain and the energy source in the evaporator heat exchanger was considered thein the interval 12:00–1:00 pm, to study the thermodynamic state change in the ORC.

Table 1 shows the main thermo-physical and environmental properties of the fluids considered in this work. It is pertinent to emphasize that there is no fluid that meets all the criteria under particular operating conditions. However, there are guidelines that serve as a guide for the selection of fluids for certain applications. Generally speaking, the working fluids with the critical temperature approaching the heat source temperature own the highest thermodynamic performance. However, although Toluene, Cyclohexane, and Acetone are suitable for the heat source temperature higher than 600 K they have low Global Warming Potential (GWP) and low Ozone Depletion Potential (ODP), which makes them good candidates since environmental considerations are a factor in this study.

Table 2. Baseline input data used in the analysis of a solar-powered organic Rankine cycle system.

Configuration	Parameter	Value	Unit	Source
Solar-ORC	Turbine isentropic efficiency	80	%	[37]
Solar-ORC	Pumps isentropic efficiency	80	%	[34]
Solar-ORC	Cooling water temperature (T7)	20	°C	[38]
Solar-ORC	Pinch Point condenser	15	°C	[39]
Solar-ORC	Pinch Point evaporators	40	°C	[40]
Solar-ORC	Condensation temperature (T1)	40	°C	[41]
Solar-ORC	Pressure ratio pump 1 (P2/P1)	6		[14]
Solar collector	Pressure ratio pump 2 (P5a/P5)	2.5		[39]
Solar collector	Pressure ratio pump 3 (P9a/P9)	2.5		[39]
Solar collector	Initial tank temperature	120	°C	[42]
Solar collector	Collector inlet temperature (T10)	80	°C	[43]
Solar collector	Collector area	100	m^2	[44]
Solar collector	Overall Storage Tank Heat Transfer Coefficient $(UA)_s$	11.1	W/K	[43]

2.2. Thermodynamic analysis

The input values used for the calculation are denoted in Table 2. The exergetic and energy analyses of the system were carried out by combining the analyses of each subsystem, based on the principle of balancing exergy and energy for a control volume, assuming that each component of the system is considered as a control volume [31]. To simplify the theoretical analysis of the system, the following general assumptions were made [34]:

- Each component is considered as an open system working in a steady-state condition.
- Kinetic and potential energy changes are not considered.

Table 1. Thermo-physical and environmental properties of the selected fluids.

Working Fluid	Type	P_{crit} [MPa]	T_{crit} [°C]	NFPA 704		ALT [yr]	ODP	GWP
				Flammability	Health Hazard			
Cyclohexane	Dry	3.06	235	3	2	-	0	Low
Toluene	Dry	4.13	319	3	2	0.007	0	2.7
Acetone	Isentropic	3.78	235	3	2	-	0	0.5

- All components are well-isolated, so all processes are considered to be adiabatic.
- Pressure losses are neglected.
- Ambient temperature is set at 25 °C, and the ambient pressure is 101.3 kPa.
- Efficiencies of the pumps and the turbine are assumed constant.
- Solar collector type used is an evacuated tube collector [35], which an Eco-indicator 99 of 15300 mPts/kg for a 1m^2 [36].

The mass balance is expressed according to Eq. (1), where $\dot{m}_{in}$ is the incoming mass flow and $\dot{m}_{out}$ is the outgoing mass flow in kg/s.

$$\sum \dot{m}_{in} - \sum \dot{m}_{out} = 0 \tag{1}$$

Taking into account the first law of thermodynamics and considering the system in a steady-state condition, the overall energy balance of the system components can be calculated according to Eq. (2).

$$\dot{Q}_{cv} - \dot{W}_{cv} + \sum \dot{m}_{in} \cdot h_{in} - \sum \dot{m}_{out} \cdot h_{out} = 0 \tag{2}$$

where $\dot{Q}_{cv}$ represents the heat transfer rate to the control volume in kW, $\dot{W}_{cv}$ represents the work done by the control volume in kW, $\dot{m}$ and h represent the mass flow rate in kg/s and the specific enthalpy in kJ/kg·K of the currents that exceed the limits of the control volume, respectively.

The heat received by the solar collector $\dot{Q}_u$ that is transferred to the ORC system is calculated through the solar collector energy balance equation, based on the efficiency of the collector, as expressed in Eq. (3).

$$\dot{Q}_u = I_{TH} \cdot \eta_c \cdot A_c \tag{3}$$

where I_{TH}, η_c and A_c are the total solar irradiance affecting the collector surface in Wm^2, the instantaneous collector efficiency, and the collector area in m^2, respectively.

For the case study developed in this document, we used the Bird and Hulstrom model to determine the total ITH radiation as a result of the sum of the direct solar radiation IDH and the diffuse solar radiation IdH as shown in Eq. (4), all three terms in W/m^2.

$$I_{TH} = I_{DH} + I_{dH} \tag{4}$$

Direct solar radiation is determined by considering different cloudiness indexes, Eq. (5).

$$I_{DH} = [0.9662 \times C \times \tau_{CTA}] \sin A \tag{5}$$

where the factor 0.9662 is the correction factor that adjusts for wavelengths from 0.3 to 3μm of the solar spectrum, C is the solar constant in Julian days in W/m^2, τ_{CTA} is the atmospheric transmissibility coefficient and A is the solar altitude in degrees. In contrast, the diffuse solar radiation is calculated by the sum of the diffuse radiation due to scattering by air molecules I_{dr} the diffuse radiation due to the presence of aerosols I_{da}, diffuse radiation due to reflection from the surface I_{dm}, as shown in Eq. (6), all in W/m^2 [30].

$$I_{dH} = I_{dr} + I_{da} + I_{dm} \tag{6}$$

Instantaneous collector efficiency is defined as the ratio of useful heat gain over a specified time to the solar energy incident at the same time. It is obtained with Eq. (7) [43].

$$\eta_c = F_R \cdot (\tau \cdot \alpha) - F_R \cdot U_L \cdot \frac{(T_{f,in} - T_a)}{I_{TH}} \tag{7}$$

where F_R is the collector heat removal factor, it is calculated as the ratio of the actual heat transfer rate to the working fluid and the heat transfer rate at the minimum temperature difference between the environment and the collector absorber element. The transmittance τ, is the fraction of the incident solar radiation transmitted by the collector cover plates, in other words, the transmissibility of the collector, the absorbability α, is the fraction of the incident solar radiation absorbed by the collector element or absorbability of the collector, U_L is the overall heat loss coefficient of the collector, also known as conduction and radiation loss in W/m^2 ·°C, T_a is the ambient temperature and $T_{f,in}$ is the fluid inlet temperature to the collector. Commonly, the products $F_R \cdot (\tau \cdot \alpha)$ and $F_R \cdot U_L$ represent the characteristics of a particular solar collector and determine its performance. These values are obtained from the collector performance test data of the graph η_c vs $\frac{(T_{f,in} - T_a)}{I_{TH}}$ in which $F_R \cdot (\tau \cdot \alpha)$ is the intercept, and $F_R \cdot U_L$ is the slope [45, 51].

The system modelled in this work consists of a heat storage tank as described above. To simplify the model and obtain Eq. (8) for the energy balance, it is assumed that the fluid in the storage tank is completely mixed with the fluid coming from the collector.

$$\left[(m_{tf} \cdot C_{ptf})_s\right] \cdot \frac{dT_s}{dt} = \dot{Q}_u - \dot{Q}_{load} - (UA)_s \cdot (T_s - T_a) \tag{8}$$

where $(m_{tf} \cdot C_{ptf})_s$ is the product of the mass m_{tf} in kg of the fluid at the storage tank, and the specific heat capacity of the fluid C_{ptf} in kJ/kg·K, $\dot{Q}_u$ represents the useful heat gain of the solar collector, $\dot{Q}_{load}$ is the energy needed for the ORC system in kW, $(UA)_s$ is the product of the area of the storage and the tank loss coefficient, it is assigned a value of 11.1 W/K [43], T_s is the temperature of the fluid in the storage tank and T_a is the ambient temperature. If the tank losses, $\dot{Q}_u$ *y* $\dot{Q}_{load}$ are assumed to be constant over some time Δt, Eq. (8) can be written as Eq. (9) for each time interval.

$$T_{s,\,new} = T_s + \frac{\Delta t}{m_{tf} \cdot C_{ptf}} \cdot [\dot{Q}_u - \dot{Q}_{load} - (UA)_s \cdot (T_s - T_a)] \tag{9}$$

where $T_{s,\,new}$ is the temperature of the fluid in the storage tank at the end of the time interval Δt.

The exergy destruction rate for a steady-state control volume for each system component is as indicated in Eq. (10) [46], wherefrom left to right the first term is the exergy of heat, which is transferred at a constant temperature, the second term is the transfer of mechanical work from or to the system, the third term is the sum of the exergy input, the next is the sum of the exergy output from the system and the last is the exergy destruction rate [47]. The subscript k is the location, T is the temperature in K, and ψ is the exergy flow in kJ/kg.

$$\sum \left(1 - \frac{T_0}{T_k}\right) \cdot \dot{Q}_k - (\dot{W}) + \sum_{in} \dot{m} \cdot \psi - \sum_{out} \dot{m} \cdot \psi = \dot{E}_{xd} \tag{10}$$

According to the initial considerations of neglecting potential energy and kinetic energy, the exergy of the physical flow per unit mass for the fluid flow can be defined as in Eq. (11) [48]:

$$\psi = (h - h_0) - T_0 \cdot (s - s_0) \tag{11}$$

where s and h are the entropy and specific enthalpy both in kJ/kg·K and kJ/kg respectively, in turn, s_0 and h_0 are the entropy and specific enthalpy at ambient temperature.

The contribution of global exergy to the solar-ORC system is the exergy of the solar radiation falling on the solar collector and is a function of the external temperature of the sun ($T_s = 6000\ K$) and is defined by Eq. (12) [49].

$$\dot{E}_{in} = A_c \cdot I_{TH} \cdot \left[1 + \frac{1}{3} \cdot \left(\frac{T_0}{T_s}\right)^4 - \frac{4}{3} \cdot \left(\frac{T_0}{T_s}\right)\right] \tag{12}$$

The relationship of the irreversibility of the components of the solar-ORC system is defined as the relationship between the exergy destroyed in each component and the total loss of exergy of the system, as can be seen in Eq. (13) [50].

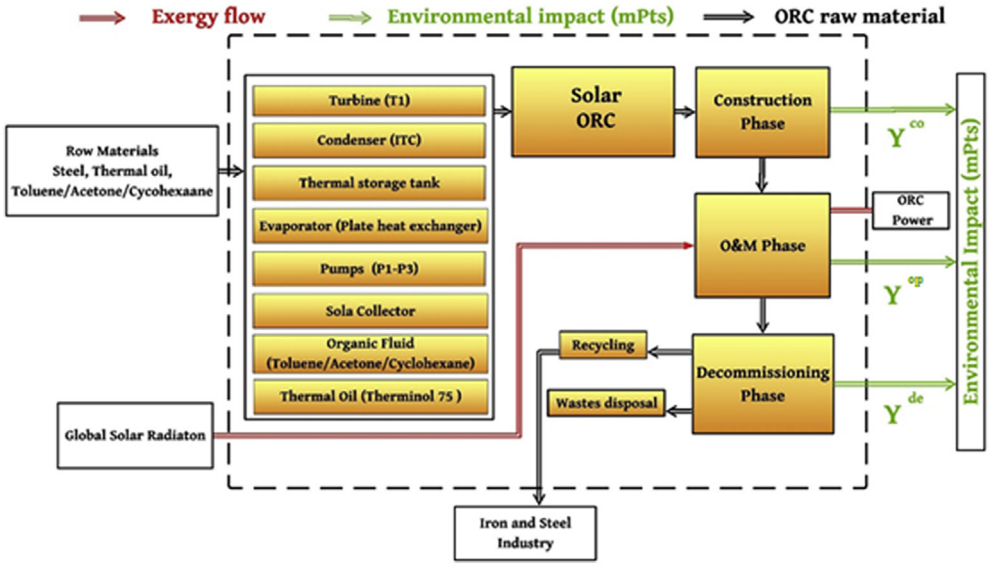

Figure 3. Assumed limits for the solar-ORC system LCA.

$$IR = \frac{\dot{E}_{xd}}{\dot{E}_{xd,\ total}} \tag{13}$$

The total loss of exergy is the sum of the loss of exergy of each component. The exergetic fuel depletion ratio (FDR) of a particular component can be defined as the relationship between the exergy destruction of each component (rate of exergy lost due to irreversibilities) and that of the overall exergy inputs to the system, as defined by Eq. (14) [50].

$$FDR = \frac{\dot{E}_{xd}}{\dot{E}_{x,\ in}} \tag{14}$$

The electrical power consumed by a pump is calculated as follows in Eq. (15).

$$\dot{W}_p = \frac{\dot{m}_{wf} \cdot v_{in} \cdot (W_{out} - W_{in})}{\eta_p \cdot \eta_M} = \frac{\dot{m}_{wf} \cdot (h_{out} - h_{in})}{\eta_M} \tag{15}$$

$\dot{m}_{wf}$ is the mass flow rate of the working fluid in kg/s, η_p, and η_M are the efficiencies of the pump and the efficiency of the electric motor, respectively. The heat transferred by the thermal oil to the working fluid in the evaporator in kW is calculated according to Eq. (16).

$$\dot{Q}_e = \dot{m}_{wf} \cdot (h_{out} - h_{in}) = \dot{m}_{tf} \cdot C_{ptf} \cdot (T_{e,in} - T_{e,out}) \tag{16}$$

where $T_{e,in}$ is the thermal oil temperature at the evaporator inlet and $T_{e,out}$ at the outlet. The electrical power generated by the turbine in kW is given by Eq. (17).

$$\dot{W}_t = \dot{m}_{wf} \cdot (h_{in} - h_{out}) \cdot \eta_g \tag{17}$$

where η_g is the efficiency of the generator. The net output power generated by the solar-ORC system is defined by Eq. (18).

$$\dot{W}_{net} = \dot{W}_t - \sum \dot{W}_p \tag{18}$$

The thermal efficiency of the solar-ORC system is given by Eq. (19).

$$\eta_{thORC} = \frac{\dot{W}_{net}}{\dot{Q}_e} \tag{19}$$

The efficiency of the whole system is defined by Eq. (20).

$$\eta_{thsys} = \frac{\dot{W}_{net}}{\dot{Q}_u} \tag{20}$$

Finally, the exergetic efficiency of the system is defined by Eq. (21).

$$\eta_{exer} = \frac{\dot{W}_{net}}{\dot{E}_{in}} \tag{21}$$

2.3. Life cycle assessment in the solar-ORC system

The selected methodology used to study the Life Cycle Assessment or Life Cycle Analysis (LCA) follows the guidelines of the ISO 14040 [51], and its objective is to determine the opportunities for improvement concerning the carbon footprint corresponding to the solar-ORC system. Specifically, the Eco-Indicator 99 method was used to evaluate the environmental impact of the thermal system.

The study considers the different phases of assembly of the materials, the construction phase of the cycle sections, the operation and maintenance stages, and the dismantling of the equipment, as it is illustrated in Figure 3. The environmental impact of the thermal oil (Therminol 75), which is composed of 73.5% diphenyl oxide, and the organic working fluids (Toluene, Cyclohexane, and Acetone) were also considered during the three phases mentioned above. Concerning the organic working fluid in the installation stage, the leak of this fluid was calculated by multiplying the power of the turbine by a factor of 5.57. During the operation, it is assumed that 10% of the organic fluid is lost, and in the dismantling phase, 3%.

By taking the evaporator and adding the sump heat exchanger, you have two plate heat exchangers to which you apply the energy balance and thus determine the required heat transfer area employing the Eq. (22) [52].

$$A_{jj'} = \frac{\dot{M}(h_j - h_{j'})}{LTD} \cdot \frac{1}{Z} \tag{22}$$

where Z is the overall heat transfer coefficient in kW/m^2·K and LTD is the average logarithmic temperature difference. Z is calculated from the local heat transfer coefficients using the Eq. (24).

$$Z = \left(\frac{1}{\alpha_{in}} + \frac{1}{\alpha_{out}} + \frac{e_w}{\lambda_w} + R_f \right)^{-1} \tag{23}$$

The indexes α_{in} and α_{out} are known or can be calculated utilizing correlations. The log means temperature difference is given by the Eq. (24) [53].

$$LTD = \frac{(T_{inj} - T_{outj}) - (T_{inj'} - T_{outj'})}{Ln\left(\frac{T_{inj} - T_{outj}}{T_{inj'} - T_{outj'}}\right)} \tag{24}$$

The actual heat transfer area A_r is calculated according to the length and width of the plates and by the number of channels. Finally, the thermal sizing of the heat exchanger is defined as the ratio between the required heat transfer area and the actual heat transfer area.

Some heat transfer and pressure laws are necessary to evaluate the design method. These laws are defined according to the flow condition (single-phase, multiphase, steam, and condensation flows). For single-phase flows, it has been determined that the main geometric parameter is the angle of corrugation. Eqs. (25) and (26) show some correlations as a function of the angle of corrugation, using Reynolds' number and Prandtl's number.

$$Nu = a \cdot Re^{b} \tag{25}$$

$$Pr^{c} = \frac{\alpha \cdot d_h}{\lambda} \tag{26}$$

where $0.1 < a < 2$, $0.6 < b < 0.8$, and $0.3 < c < 0.4$.

When the flow is in the steam phase, an annular flow pattern has been adopted for most applications due to the high heat transfer coefficient obtained from this pattern. As in shell and tube exchangers, two phenomena occur in this type of arrangement: convective boiling (cv) and nucleated boiling (nb), the latter being important for very high heat flows or low mass flows, and its heat transfer coefficient is a function of the heat flow and the properties of the fluid, using Cooper's correlation [54] for its estimation as can be seen in Eq. (27).

$$\alpha_{nb} = -55 \cdot M^{-0.5} \cdot P_s^{0.12} \cdot \dot{q}^{0.67} \cdot log_{10}^{-0.55}(P_s) \tag{27}$$

Convective boiling is estimated using an enhancement factor F which is due to the enhancement of heat transfer caused by the influence of liquid vapour. Therefore, convective boiling is calculated according to Eq. (28).

$$\alpha_{cv} = F \cdot \alpha_L \tag{28}$$

where α_L is the liquid heat transfer coefficient, and for its calculation, the appropriate correlations for corrugated channels are used, as shown in Eq. (29).

$$\alpha_L = a \cdot \left[\frac{\dot{m} \cdot (1-x) \cdot d_h}{\mu_L}\right]^{b} \cdot \left(\frac{\mu_L \cdot c_{pL}}{\lambda_L}\right)^{c} \cdot \frac{\lambda_L}{d_h} \tag{29}$$

The improvement factor F is calculated according to Eq. (30).

$$F = 1 + \frac{1.8}{X_{tt}^{0.79}} \tag{30}$$

where X_{tt} is the Lockhart-Martinelli number, which is determined by Eq. (31).

$$X_{tt} = \left(\frac{1-x}{x}\right)^{0.9} \cdot \left(\frac{\rho_G}{\rho_L}\right)^{0.5} \cdot \left(\frac{\mu_L}{\mu_G}\right)^{0.1} \tag{31}$$

The highest value term between nucleated and convective boiling is chosen as the two-phase heat transfer coefficient.

For condensation, it has been shown that two condensation regimes are depending on the mass flow, if the mass flow is low ($Re < 1000$), it is considered gravity controlled regime, and it is assumed that the liquid is separated from the vapor, and for high mass flows it is considered shear controlled regime and a turbulent model is assumed. In the first regime, Nusselt's theory underestimates the heat transfer coefficient by a factor of two to three because the liquid film drains into the corrugation trenches. For the second regime, the correlations are based on the heat-moment analogy, determining that the heat transfer coefficient corresponds to the heat transfer coefficient of the condensed liquid, as can be seen in Eq. (32).

$$\alpha = \alpha_{Lo} \cdot \left[1 + x \cdot \left(\frac{\rho_L}{\rho_G} - 1\right)\right]^{0.5} \tag{32}$$

where α_{Lo} is calculated according to Eq. (33).

$$\alpha_{Lo} = a\left(\frac{\dot{m} \cdot d_h}{\mu_L}\right)^{b} \cdot \left(\frac{\mu_L \cdot c_{pL}}{\lambda_L}\right)^{c} \cdot \frac{\lambda_L}{d_h} \tag{33}$$

Although the heat transfer coefficient is disregarded for low corrugation angles and overestimated for high corrugation angles.

Due to the geometry of corrugated channel heat exchangers, the pressure drop is important, causing the saturation temperature to vary by several degrees between the inlet and outlet, affecting the average temperature difference between the hot and cold fluid. The pressure drop in two-phase flows is estimated by considering the pressure drop of the liquid flow and the gaseous flow from the correlations of the single-phase flow, as can be seen in Eqs. (34) and (35).

$$\Delta p_L = 4f_L \cdot \frac{\dot{m}^2 \cdot (1-x)^2}{2\rho_L} \cdot \frac{L}{d_h} \tag{34}$$

$$\Delta p_G = 4f_G \cdot \frac{\dot{m}^2 \cdot x^2}{2\rho_G} \cdot \frac{L}{d_h} \tag{35}$$

The mass of the heat exchanger is obtained from Eq. (36).

$$M_j = \rho \cdot A_{jj'} \cdot \beta \tag{36}$$

where ρ is the density, for copper, it is 8900 kg/m^3 and for steel 7930 kg/m^3, and β is the material thickness with a value of 0.002 m. The mass of the turbine and pumps is calculated using Eq. (37).

$$M_j = \alpha \cdot W_j \tag{37}$$

where W_i represents the power consumed by the pump and the power generated by the turbine, α is the required material quality in kg/kW, which for steel is 31.22 kg/kW for the turbine and 14 kg/kW for the pump, and for copper is 35.03 kg/kW for the turbine and 15.71 kg/kW for the pump.

The environmental impact of each component in the construction phase is calculated through Eq. (38), where w_j is the coefficient of the component Eco 99.

$$Y_j^{co} = w_j \cdot M_j \tag{38}$$

Therefore, the environmental impact of the equipment (Y_i^{LCA}) throughout its lifetime is obtained using Eq. (39).

$$Y_j^{LCA} = Y_j^{co} + Y_j^{op} + Y_j^{de} \tag{39}$$

where Y_j^{co} is the environmental impact by construction, Y_j^{op} is the environmental impact by operation and Y_j^{de} is the environmental impact by dismantling. Finally, the total environmental impact of the system components is calculated with Eq. (40).

$$Y_j = Y_j^{LCA} + Y_j^{f} \tag{40}$$

where Y_j^f refers to the influence of the volume of the fluids in each device of the system, and is a function of the exergy destruction of the component and is obtained employing Eq. (41).

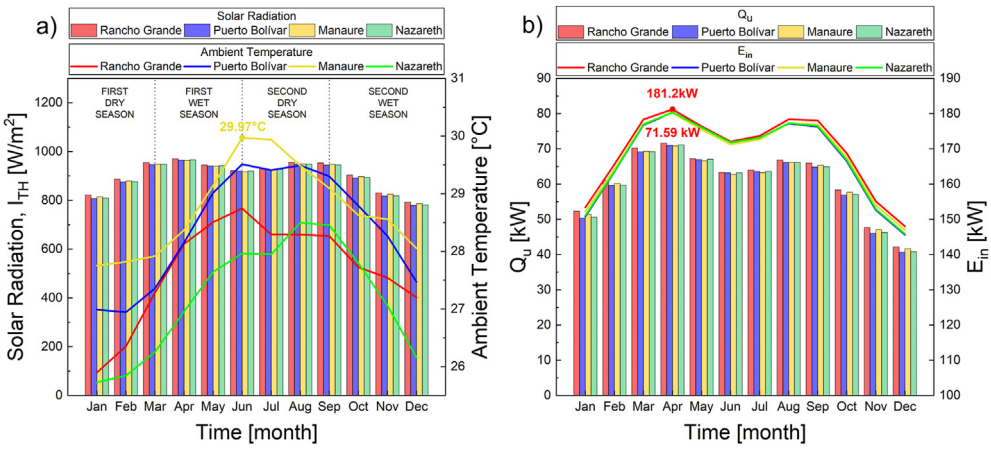

Figure 4. a) Total solar radiation and ambient temperature during one year in several stations, b) Useful heat gain and input exergy of the fluid in the thermal storage tank.

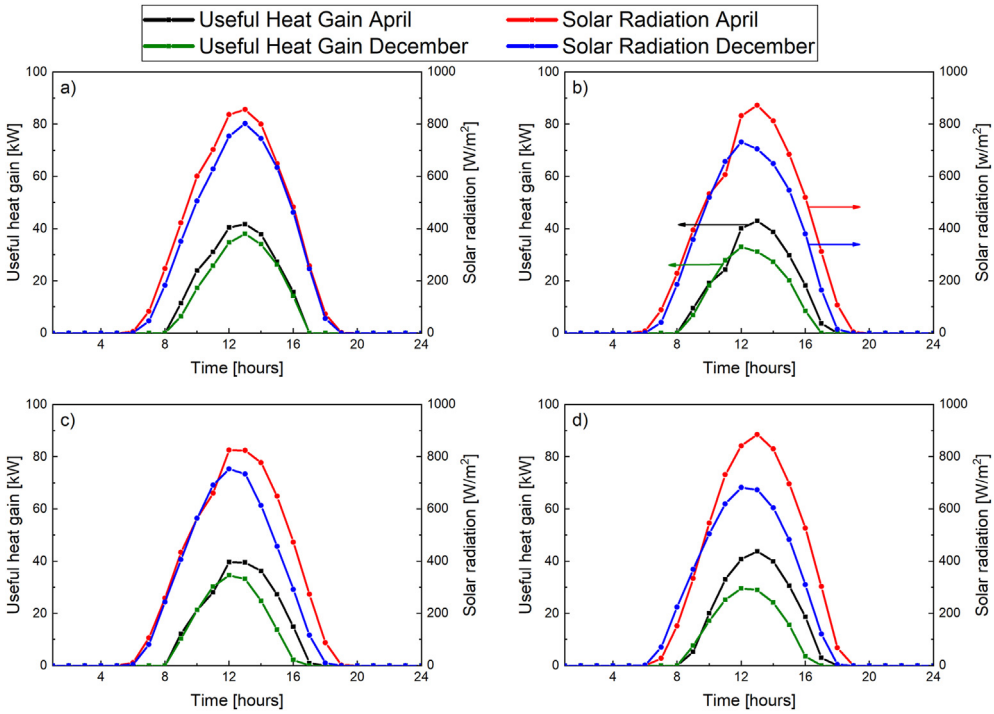

Figure 5. Maximum and minimum heat gain and maximum and minimum radiation in a day for the four study stations. a) Rancho Grande, b) Manaure, c) Nazareth, d) Puerto Bolívar.

$$Y_j^f = Y^f \cdot IR \tag{41}$$

2.4. Solar potential evaluation of proposed site

These four cities are located in the department of Guajira, Northern Colombia, as shown in Figure 6. The selection of these cities obeys the fact that these cities have the highest solar radiation registered in the area, allowing the possibility of analyzing the effects of solar radiation on the general performance of the solar-ORC system. The average room temperature was taken from 36 years data set (1983–2019) provided by IDEAM [55]. The ambient temperature affects solar efficiency, which in turn affects the amount of heat transferred to the ORC system. To simulate the system, the values in Table were used.

The corresponding total average solar radiation and ambient temperature for these cities during a period studied is presented in Figure 4a. In Figure 4b is shown the heat gained or heat introduced to the system by the solar collector during one year, and the variation of the entropy of the fluid entering the storage tank in one year are presented.

In Figure 4a is evident that the month with the highest total solar radiation is April, and this data compared to Figure 4b shows that heat gain has a direct relationship with radiation since heat gain has the same behavior during the year and in April we have the maximum value for the four cities in both cases, being the Rancho Grande station the one that receives the highest maximum radiation with 970.3 W/m^2 and therefore the highest maximum heat gain with 71.59 kW. On the other hand, Rancho Grande is the station where the highest input entropy obtains the fluid in the storage tank, reaching a peak of 181.2 kW in April, but it is not the city where the highest average temperature is presented since, in this case, it is the city of Manaure with practically 30 °C in June.

With the maximum and minimum data of radiation and heat gain shown in Figure 4, the daily calculation was made for each station in

Table 3. Proposed ORC model validation.

Working fluid	Net power output (kW)			Thermal efficiency (%)		
	Song et al. model [56]	Proposed model	Absolute error (%)	Song et al. model [56]	Proposed model	Absolute error (%)
Toluene	89.2	89.5	0.34	21.0	21.2	0.95
Cyclohexane	90.1	91.3	0.99	21.2	21.6	1.89
Benzene	90.8	89.9	0.99	21.3	20.9	1.88

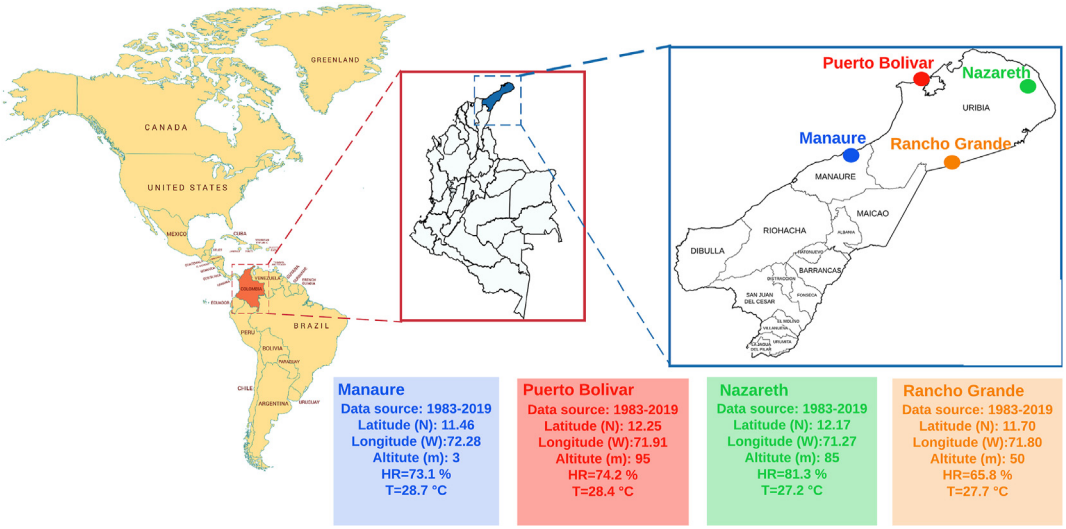

Figure 6. The geographical location of the study area.

April, which is the month where the maximum values are given, and in December for the minimum values as shown in Figure 5.

The stations average the start of solar radiation at six o'clock in the morning and end of radiation at seven o'clock at night in the maximum month, except for the Rancho Grande station, where the end of radiation coincides with both the maximum and minimum month. Similar behavior is recorded on the curve corresponding to heat gain only that the start averaged 7:30 a.m. and the end at 5:00 p.m. The rest of the results presented in this study are focused on an annual context.

3. ORC model validation

The thermodynamic model proposed for the individual ORC was validated with the results of a waste heat recovery system of a diesel engine presented by Song et al. [56], considering the Toluene, Cyclohexane, and Benzene as organic working fluids. Also, operational conditions were the pump and expander efficiency (80%), evaporator and condenser pinch point temperature (6 K), and a cooling water temperature (T_7) in 298.15 K.

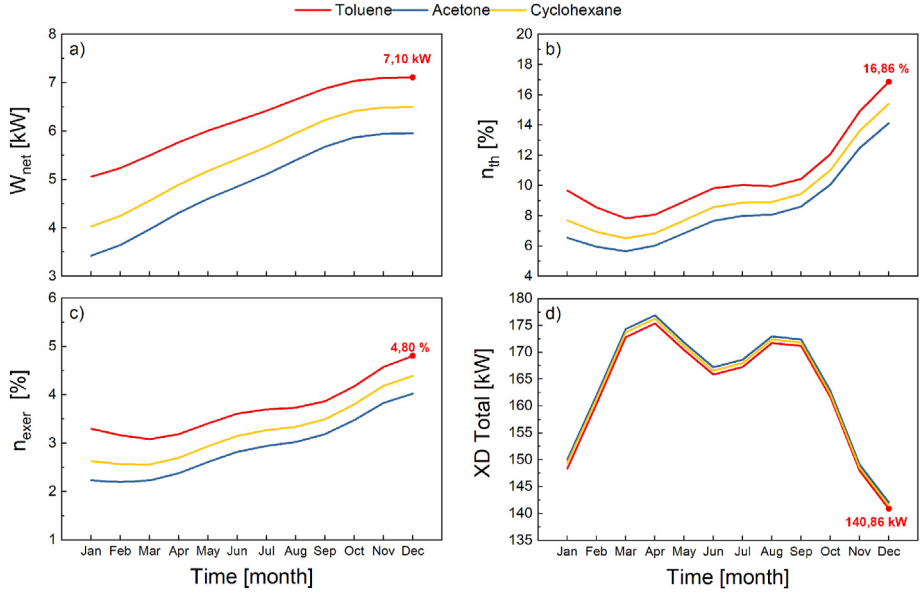

Figure 7. Thermal parameters of solar -ORC, a) Net power, b) thermal efficiency, c) exergy efficiency, and d) total exergy destroyed.

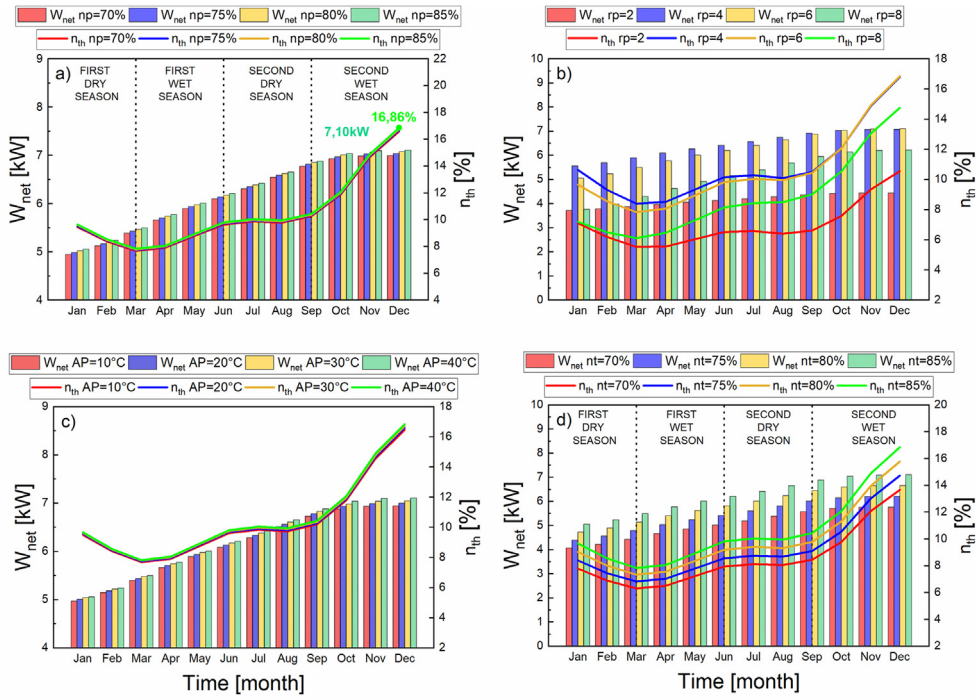

Figure 8. Net power and thermal efficiencies as function of the: a) pump efficiency, b) pressure ratio, c) evaporator pinch point temperature, and d) turbine efficiency.

The results of the validation of the proposed model are shown in Table 3 for net power output and thermal efficiency, which show a fair agreement with the values proposed by the model of Song et al. [56].

In the case of net power output, the highest absolute errors were obtained for Cyclohexane and Benzene, both error of 0.99%; while for thermal efficiency, the highest absolute error was obtained for Cyclohexane (1.89%), which is assumed as sufficient error. Thus, this model has been adopted to evaluate the thermal and exergetic performance of an ORC with the solar thermal source before different working fluids and different places of higher solar potential on the Colombian Caribbean coast.

4. Results and discussion

The energy, exergy, and environmental study of the solar-ORC performance help to determine the appropriate location of these systems in Colombia, allowing to increase their application and market penetration. To obtain the highest energy efficiency from these systems, researchers have dedicated themselves to studying the optimization of parameters in ORC systems [57] but have not considered the identification of opportunities for environmental improvement in their scope. Therefore, this section has presented the results of the numerical simulation over one year for the solar-ORC system using the mathematical models described in the methodology for the cities Rancho Grande, Puerto Bolivar, Manaure, and Nazareth. These four cities are located in the department of Guajira, Northern Colombia, as shown in Figure 6. It is expected that at the places where the solar radiation conditions are higher, the solar-ORC will have a better performance.

4.1. Thermal system performance under different working fluids

To evaluate the different efficiencies, power generated and energy destroyed by each working fluid every month for one year, data from the Rancho Grande station was taken to run the simulation. Toluene shows the highest performance concerning the other fluids as shown in Figure 9, being only important its high exergy destruction concerning the other fluids, as it could be already intuited according to the previous section. As can be seen from the work results and efficiencies measured by the monitoring stations in Figure 7, in this case, we also have the highest efficiencies in December, where Toluene has a thermal efficiency of 14.6% and an exergetic efficiency of 7.37%. In October, the greatest net power is registered with 5.5 kW while Acetone in December registers minimum exergy destruction equivalent to 92.5 kW, which is 2.5% less than that presented by cyclohexane in this aspect.

Figure 7-a reveals that the net power of the system tends to increase as the months pass. This is due to the increase in inlet temperature to the ORC evaporator due to the solar radiation incident on the collector, which is associated with the increase in radiation during the months of January through April. Note that, during the months of May, June, and July there is a decrease in the monthly average radiation values (see Figure 4-a). However, the trend of the net power of the system is increasing. This indicates that, despite a decrease in the heat absorbed in the collector, the thermal tank has gained thermal capacitance which allows it to increase its temperature up to 10 °C above its initial temperature. This is due to the volume of the tank, which causes the temperature fluctuation levels due to radiation changes to be minimal. Then, from September onwards, the temperature tends to stabilize as a result of the thermal load transferred to the ORC and the decrease in radiation levels for the months of October, November, and December.

On the other hand, regarding the thermal efficiency and exergy efficiency shown in Figure 7-b, and Figure 7-c, respectively, the data show that in January, February, and March the tendency is to decrease. This is because, although there is an increase in the net power of the system (Figure 7-a), the increase in the solar ORC input exergy (solar radiation exergy) prevails over the increase in net power. This generates a decrease in the exergy efficiency, as well as in the energy efficiency. In this sense, the behavior of the energy and exergy efficiency of the solar-ORC system exhibit an inverse behavior to the trend in the levels of incident radiation on the solar collector. That is, an increase in radiation levels (Figure 4-a), generates a decrease in the exergy and energy performance, since the increase in exergy and heat input to the solar-ORC system prevails over the increase in net power experienced by the system. The opposite case is observed when radiation decreases, in this case, power generation prevails causing an increase in these indicators. It is important to note that

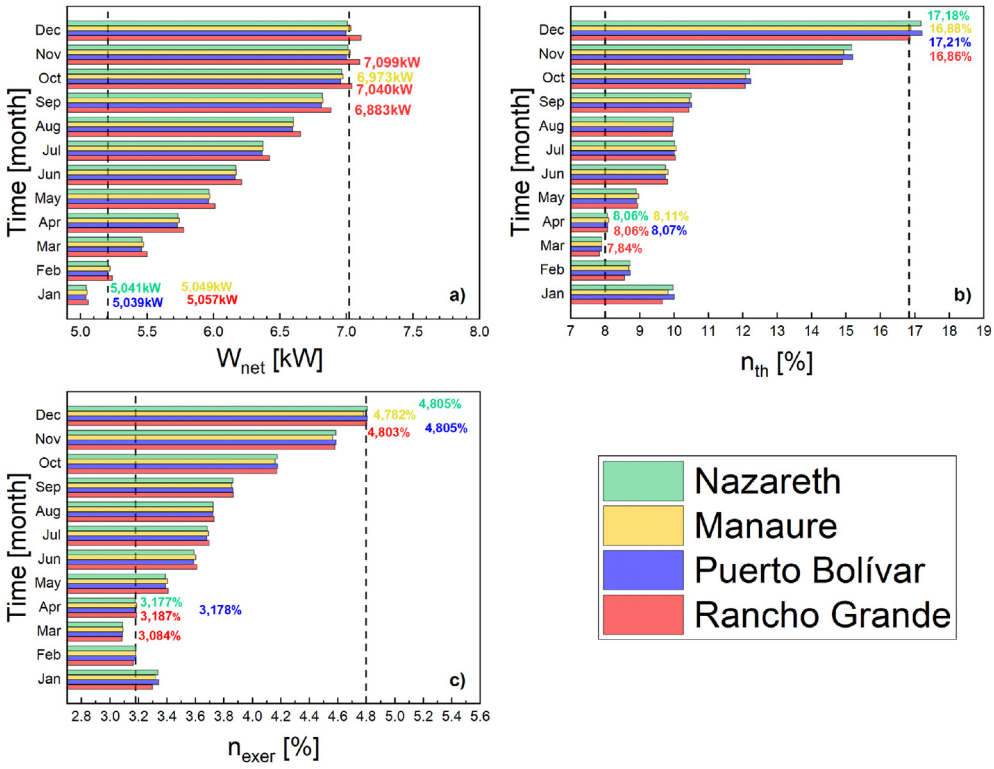

Figure 9. a) Net power generated per month, b) thermal efficiency generated per month, and c) exergy efficiency generated per month.

the exergy efficiency is lower than the energy efficiency. For example, Figure 4-b shows that the input exergy to the ORC-solar system (181.2 kW) and the input heat absorbed by the collector (71.59 kW), taking April as the base month. Under these conditions, the system is able to generate 5.77 kW of mechanical power (Figure 7-a), which implies a conversion efficiency into useful work of 3.18%; while 96.81% (175.43 kW, Figure 7-d) corresponds to internal irreversibilities of the ORC-Solar system. The energy efficiency obtained is 8.07 %.

Finally, the total exergy destroyed of the system exhibits the behavior of radiation. The higher the radiation level, the higher the total exergy destruction rate of the system. This is due to the fact that the solar collector is the equipment that destroys the most exergy due to heat transfer irreversibilities, which represents about 70.57 %.

On the other hand, some research has attempted to present a relationship between the thermal properties of the working fluids and the thermal performance of the ORC cycle. According to the results presented by Fan et al. [58] one of the main properties of the working fluids that affect the thermodynamic performance of the ORC cycle is the critical temperature (T_{cr}), which impact thermal stability during the heat transfer process in the evaporator. In this sense, toluene presents the highest critical temperature (319 °C), while Cyclohexane, and Acetone have the same value of 235 °C. Therefore, Toluene has the advantage of having a greater heat absorption capacity along the evaporator in the heating, evaporation and superheating stages. Consequently, the higher the degree of heat utilization from the thermal source due to thermal stability, the higher the energetic and exergy performance of the ORC cycle, as shown in Figure 7-b y Figure 7-c. This is due to the evaporation temperature of the fluid with high critical temperature. The higher the evaporation temperature, the higher the enthalpy difference of the working fluid in the expansion stage and, therefore, the higher the net power. In this sense, for a fixed evaporation temperature, toluene will be the fluid with the highest power production rate, as shown in Figure 7-a.

As mentioned in this document and taking into account the results shown in Figure 7, the calculation of the operational variables was simulated using Toluene as the working fluid, varying operational conditions, and using the radiation data corresponding to the Rancho Grande station to complete the calculation. For a better understanding of the results obtained, the year was divided into four seasons, two wet seasons and two dry seasons. The year begins with the first dry season from January to March, then the first wet season from April to June, followed by the second dry season from July to September, and ending with the second wet season from October to December.

Figure 8-a shows that the highest thermal efficiency of the system is obtained in December in the second wet season when the pump operates at 85% efficiency, resulting in a thermal efficiency of 16.86%. The work generated by the system varies throughout the year from 4.95 kW to 7.10 kW, which is the maximum peak at the beginning of the second wet season in October. This maximum is also given for a pump efficiency of 85%. From Figure 8-b the thermal efficiency varies from 10.63% to 16.80%, when the pressure ratio is equal to 4, which, together with the pressure ratio equal to 6, present efficiency values higher than those registered by the pressure ratio of 2 and the rp of 8 which is the one that gives the lowest thermal efficiency values. Additionally, it is observed that the highest power production rates were found for pressure ratios between 4 and 6, with source temperatures between 120 °C-130 °C. Figure 8-c shows that the power output increases as the AP increases. Similar behavior was found for thermal efficiency. This is explained by the fact that, the higher the AP, the higher the enthalpy jump in the turbine, and as a result, the higher the power production rate and the higher the thermal efficiency of the system for these particular operating conditions. The data obtained by varying the efficiency of the turbine show that increasing the efficiency increases the net power and the thermal efficiency, obtaining the highest net power in October and the highest efficiency in December; these maximum values are equal to the maximums obtained in Figure 8-a.

4.2. Annual simulation of the solar-ORC

The net power generated (Figure 9a), the thermal efficiency (Figure 9b), and the exergetic efficiency (Figure 9c) of the system were

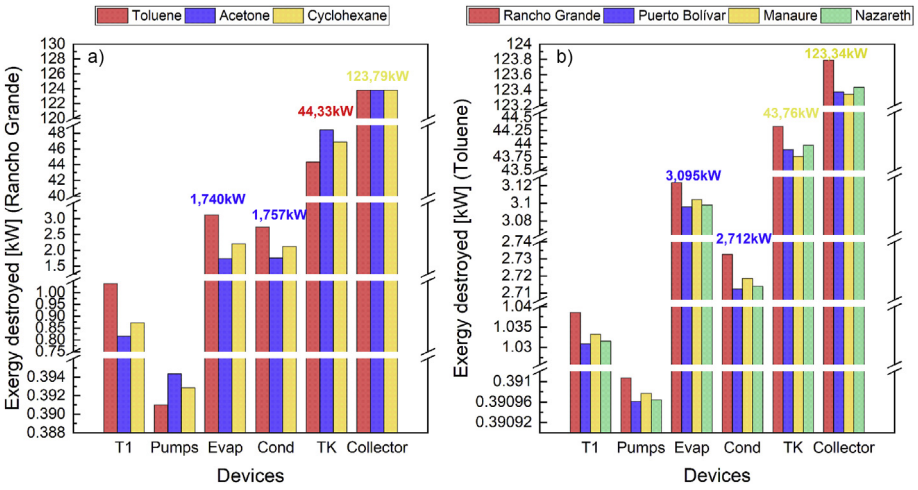

Figure 10. a) Exergy destroyed in different components for several working fluids. B) Exergy destroyed in different components for several monitoring stations.

Table 4. Solar-ORC system component's exergy analysis results.

Station		T1	Pumps	Evap	Cond	TK	Collector
Rancho Grande	IR [%]	0.59	0.22	1.78	1.56	25.27	70.57
	FDR	0.57	0.22	1.72	1.51	24.47	68.32
Puerto Bolívar	IR [%]	0.59	0.22	1.77	1.55	25.15	70.70
	FDR	0.57	0.22	1.72	1.50	24.35	68.45
Manaure	IR [%]	0.59	0.22	1.78	1.56	25.10	70.75
	FDR	0.57	0.22	1.72	1.51	24.30	68.48
Nazareth	IR [%]	0.59	0.22	1.77	1.55	25.18	70.68
	FDR	0.57	0.22	1.72	1.50	24.38	68.43

studied monthly. The maximum net power is presented at the Rancho Grande station between September, October, and November, with the peak in November at 7.09 kW, while the minimum work was recorded in the first months of the year, especially at the Puerto Bolivar and Nazareth stations, where the minimum work is 5.039 kW at the Puerto Bolivar station.

Contrary to the characteristic of the net power data, the thermal efficiency of the solar-ORC in January also registers high values, besides in December is where the maximum peaks of thermal efficiency are registered, which for this case are presented in the cities of Puerto Bolivar and Nazareth, where the maximum among them is in the city of Puerto Bolivar where a 17.21% efficiency is registered. On the other hand, the minimum values are registered in April, and Mach but in this case, the minimum value is given in the city of Rancho Grande with an efficiency of 7.84%. A behavior very similar to the graph of the thermal efficiency presents the graph of the exergetic efficiency wherein the same way in December the maximum values are generated in the city of Puerto Bolivar (4.80%), Rancho Grande (4.80%), and Nazareth (4.80%). The lowest efficiency in March, and April in Rancho Grande registering an efficiency of 3.08%, and 3.18%. Although the minimum values for both efficiencies are presented in March, April the system is still capable of generating energy.

4.3. Exergy analysis results

This section presents the results obtained from the exergy analysis that was carried out through the exergetic evaluation that was performed on each component of the system. The analyzed parameters in this section were: exergy destroyed shown in Figure 10, exergetic depletion fuel (FDR), and the radius of irreversibility (IR), both tabulated in Table 4, also the results corresponding to the Rancho Grande station for the April month from 12:00 pm to 1:00 pm, which is the period with the largest solar radiation and power generated. Figure 10-a shows that the solar collector is the equipment with the highest rate of exergy destruction (123.79 kW-70.57 %), followed by the thermal tank (44.33 kW-25.27% with toluene). For the heat exchange equipment, the rate is low compared to that found for the thermal tank and solar collector. While for the pumps (pump1, pump2, and pump3) they represent a low percentage. Therefore, efforts should be oriented towards the reduction of irreversibilities in the collector and in the thermal tank. Of the fluids considered in this article, Toluene is the most widely used fluid in ORC systems and with industrial applications in operation [41] for which reason Toluene was considered as a working fluid for each station.

Figure 10-b shows the results of exergy destroyed at each station for the components that make up the system, and the amount of exergy destroyed is similar to those presented by the analysis of exergy destroyed by each working fluid. By minimal differences, the Manaure station is the station that destroys the least exergy, and the Puerto Bolivar station is the station that records the least exergy destruction in terms of the storage tank, condenser, and evaporator. The exergy destroyed by the evaporator only represents 1.77% of the exergy destroyed by ORC-solar. This large amount of exergy that destroys the collector is attributed to the large temperature difference present in the collector, while the mixture between the fluids of different temperatures in the storage tank is the main cause of loss of exergy in this device.

For the calculation of Table 4, the data corresponding to the total radiation for April in which the maximum radiation values are obtained was taken, and Toluene was used as the working fluid for the same reasons as those given for the calculation of part b of Figure 10.

The irreversibility ratio identifies the relationship between the total exergy loss and the exergy destroyed in the system. For this reason, and following the results already shown in Figure 10, in Table 4, it can be seen that the highest IR for all four stations is obtained in the collector. Due to the characteristics of the current technology of the solar collectors, avoiding the loss of exergy in this type of device is almost unavoidable. For the case of the storage tank, important values of these indicators were presented because it was modeled as a heat exchanger, where the exergy destroyed is a function of the temperature differences between the currents. On the other hand, the heat exchange equipment of the ORC (condenser and evaporator) represents 3.34% of the total exergy destroyed in the system. This percentage is associated to the increase of entropy inside the devices due to the temperature difference between the fluids, which results in a decrease of the useful work and, therefore, a higher exergy destruction rate. Next, the three pumps represent 0.22% which is due to the fact that this equipment are the ones with the lowest power in the proposed system and, therefore their low impact on the global inefficiency of the system.

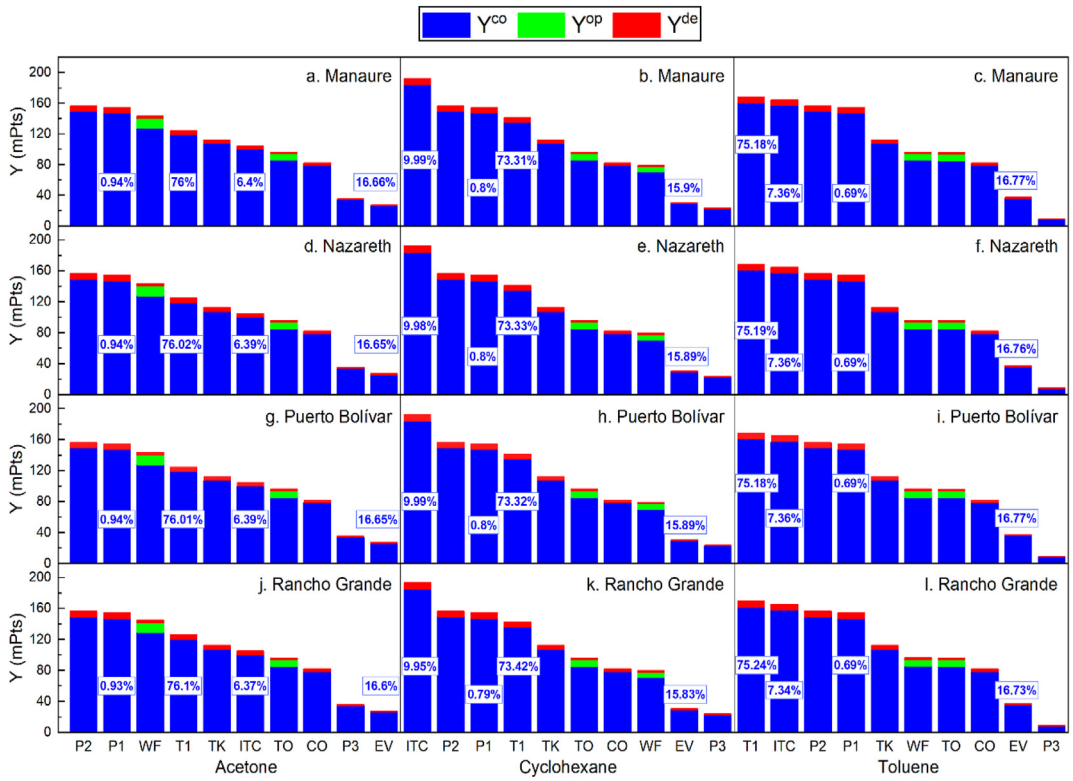

Note: the scale considered was: $Y_{CO} \cdot 10^6$, $Y_{TO} \cdot 10^5$, $Y_{TK} \cdot 10^4$, $Y_{WF} \cdot 10^3$, Y_{T1} and $Y_{EV} \cdot 10^2$, and $Y_{ITC} \cdot 10$.

Figure 11. Environmental impact of each component concerning organic fluids and location, using steel as a construction material. Note: the scale considered was: $Y_{CO} \cdot 10^6$, $Y_{TO} \cdot 10^5$, $Y_{TK} \cdot 10^4$, $Y_{WF} \cdot 10^3$, Y_{T1} and $Y_{EV} \cdot 10^2$, and $Y_{ITC} \cdot 10$.

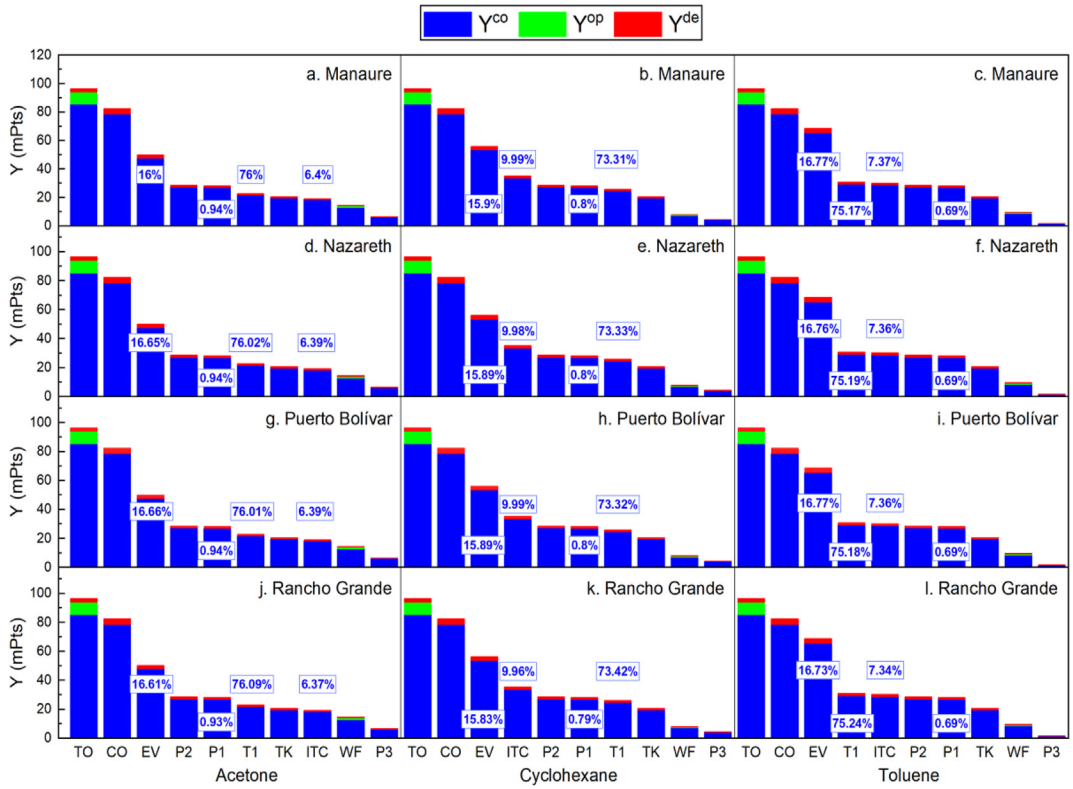

Note: the scale considered was: Y_{CO} and $Y_{TK} \cdot 10^6$, $Y_{TO} \cdot 10^5$, Y_{WF}, Y_{EV}, Y_{ITC}, and $Y_{T1} \cdot 10^4$, Y_{P1}, $Y_{P2,}$ and $Y_{P3} \cdot 10^2$

Figure 12. Environmental impact of each component concerning organic fluids and location, using cooper as a construction material. Note: the scale considered was: Y_{CO} and $Y_{TK} \cdot 10^6$, $Y_{TO} \cdot 10^5$, Y_{WF}, Y_{EV}, Y_{ITC}, and $Y_{T1} \cdot 10^4$, Y_{P1}, $Y_{P2,}$ and $Y_{P3} \cdot 10^2$.

The exergetic fuel depletion ratio (FDR) is another parameter that indicates the exergy destruction ratio compared to the exergy entering the system. In Table 1 and following the line of this section, the solar collector is again confirmed as the element that destroys the most exergy. Under the parameters of the FDR, on average, the collector destroys close of 70%% of the exergy input. The devices that destroy the least exergy are the pumps present in the system (0.22%)

4.4. Life cycle assessment

The masses of the fluids used in the solar-ORC system in the different phases of the process life cycle were calculated for each location, and the inventory for the construction of a 1 m^2 flat plate solar collector was considered [36]. The metal materials that make up the construction of the solar collector are considered primary, i.e., first-time use and not from recycling systems.

Figure 11 shows the environmental impact of each system component after performing the life cycle analysis in the three process phases, production, operation and maintenance, and decommissioning. Steel is the material used to manufacture the components. Figure 12 shows the results of using copper to manufacture the system components.

In the twelve configurations presented in Figure 11 the solar collector is the component with the highest total environmental impact 78557850 mPts, while the thermal oil is the fluid that most impacts the environment 8549928 mPts, it should be mentioned that the heat storage tank because it also has a high environmental impact with 1074118.50 mPts, on the contrary, the pump 3 is the component with the lowest environmental impact. As far as the ORC is concerned, the turbine is the component with the highest environmental impact, at 76%, compared to the other components where the pump is the component with the lowest impact, representing only 0.93%. In general terms, in the Rancho Grande location, the turbine has a greater impact than the other components of the ORC system, and at the same time, in the Rancho Grande location, it is the location with the greatest environmental impact per component in contrast to Manaure, which has the least environmental impact per component.

Unlike the results obtained with steel as a construction material, when copper is used, the heat storage tank becomes the second most influential component in the environmental impact of the system, surpassing the thermal oil, reaching 19624500 mPts. The turbine is now more important than the working fluid, with 295516 mPts over 129026 mPts in its maximum values registered in the town of Rancho Grande. The percentage influences are maintained, and Rancho Grande continues to be the location where the components register the greatest environmental impact, as well as the location of Manaure where the values of less environmental impact are registered.

As far as the influence of the working fluid is concerned, for both the steel and copper configuration, the highest environmental impacts are recorded when using Toluene as working fluid, while the lowest environmental impacts are recorded with Acetone as working fluid. For example, the evaporator using Toluene at the Nazareth location has an environmental impact of 3584.18 mPts and 65484 mPts with steel and copper respectively, but using Acetone at the same location the environmental impact drops to 2608.67 mPts and 47661 mPts for steel and copper respectively.

5. Conclusion

A solar powered ORC was studied in this document with radiation data from meteorological monitoring stations in four cities of the Guajira department, Colombia. Coupling between the solar system and the ORC is done using a storage tank that operates during non-radiation hours. It was analyzed the influence of solar radiation every month and the influence of working fluids on system performance. An exergetic analysis was also performed to analyze the behavior of each system component concerning each working fluid and the radiation data from each monitoring station.

Of the monitoring stations studied in this document, the one that records the highest radiation values was the Rancho Grande monitoring station, where the best values for power generation are also obtained.

Of the three fluids analyzed, Toluene was the fluid that showed the best results. Toluene had the highest net power, a maximum of 5.5 kW, the best exergetic efficiency with 7.37%, and the best thermal efficiency of the system, reaching a peak of 14.6%.

In the exergetic analysis, it was determined that the solar collector is the device that destroys the most exergy. However, due to the current technology no many improvements can be made. Nevertheless, as the storage tank is the second device with the highest exergy destruction, it becomes the most interesting device to be improved.

The output power generation and thermal efficiency of the solar powered ORC was also studied by a sensibility analysis. This study revealed the preference of a lower evaporator pinch point temperature, higher turbine thermal efficiency, pump thermal efficiency, and pressure ratio to obtain better energy and exergy efficiency of the solar powered ORC system.

Life Cycle Analysis to evaluate the environmental impact of each component when the three fluids used solar powered ORC. The environmental impact of the storage tank appears with 19624500 mPts, followed by the thermal oil with 8549928 mPts, these two, remain unchanged. That is to say, they are not affected by the location and the working fluid.

This manuscript only presents an energetic, exergetic, and environmental study of an ORC system coupled to a solar system. For future research, it is recommended to perform thermo-economic and multi-objective optimization studies considering the tank volume and the solar collector area as decision variables on the exergy and economic performance to reach a break-even point.

Declarations

Author contribution statement

Geanette Polanco Piñerez: Conceived and designed the experiments; Performed the experiments; Contributed reagents, materials, analysis tools or data; Wrote the paper.

Guillermo Valencia Ochoa: Conceived and designed the experiments; Performed the experiments; Analyzed and interpreted the data; Wrote the paper.

Jorge Duarte-Forero: Conceived and designed the experiments; Contributed reagents, materials, analysis tools or data; Wrote the paper.

Funding statement

This work was supported by Vicerrectoría de Investigaciones, Extensión y Proyección Social from the Universidad del Atlántico, with the grand ING82-CII2019.

Data availability statement

The data that has been used is confidential.

Declaration of interests statement

The authors declare no conflict of interest.

Additional information

No additional information is available for this paper.

References

[1] A. Shahsavari, M. Akbari, Potential of solar energy in developing countries for reducing energy-related emissions, Renew. Sustain. Energy Rev. 90 (Jul. 2018) 275–291.

[2] R.B. Jackson, P. Friedlingstein, R.M. Andrew, J.G. Canadell, C. Le Quéré, G.P. Peters, Persistent fossil fuel growth threatens the Paris Agreement and planetary health, Environ. Res. Lett. 14 (12) (Dec. 2019) 121001.

[3] İ. Dinçer, C. Zamfirescu, Sustainable Energy Systems and Applications, Springer, US, 2012.

[4] Y.S. Mohammed, M.W. Mustafa, N. Bashir, Status of renewable energy consumption and developmental challenges in Sub-Sahara Africa, Renew. Sustain. Energy Rev. 27 (Nov. 2013) 453–463.

[5] G.K. Singh, Solar power generation by PV (photovoltaic) technology: a review, Energy 53 (May 2013) 1–13.

[6] J. Abdulrahman, et al., Investment Opportunities in West Africa: Suitability Maps for Grid-Connected and Off-Grid Solar and Wind Projects, 2016.

[7] N.K. Sharma, P.K. Tiwari, Y.R. Sood, Solar energy in India: strategies, policies, perspectives and future potential, Renew. Sustain. Energy Rev. 16 (1) (Jan. 2012) 933–941.

[8] T. Tartière, A world overview of the organic rankine cycle market, Energy Procedia 129 (Sep. 2017) 2–9.

[9] S. Quoilin, M. Orosz, H. Hemond, V. Lemort, Performance and design optimization of a low-cost solar organic Rankine cycle for remote power generation, Sol. Energy 85 (5) (May 2011) 955–966.

[10] A. Schuster, S. Karellas, E. Kakaras, H. Spliethoff, Energetic and economic investigation of organic rankine cycle applications, Appl. Therm. Eng. 29 (8–9) (2009) 1809–1817.

[11] E. Spayde, P.J. Mago, Evaluation of a solar-powered organic Rankine cycle using dry organic working fluids, Cogent Eng. 2 (1) (Dec. 2015) 1085300.

[12] K.-C. Pang, T.-C. Hung, Y.-L. He, Y.-Q. Feng, C.-H. Lin, K.-W. Wong, Developing ORC engineering simulator (ORCES) to investigate the working fluid mass flow rate control strategy and simulate long-time operation, Energy Convers. Manag. 203 (Jan. 2020) 112206.

[13] W. Sun, X. Yue, Y. Wang, Exergy efficiency analysis of ORC (Organic Rankine Cycle) and ORC-based combined cycles driven by low-temperature waste heat, Energy Convers. Manag. 135 (Mar. 2017) 63–73.

[14] S.-C. Yang, T.-C. Hung, Y.-Q. Feng, C.-J. Wu, K.-W. Wong, K.-C. Huang, Experimental investigation on a 3 kW organic Rankine cycle for low-grade waste heat under different operation parameters, Appl. Therm. Eng. 113 (Feb. 2017) 756–764.

[15] K.-C. Pang, et al., Experimental study on organic Rankine cycle utilizing R245fa, R123 and their mixtures to investigate the maximum power generation from low-grade heat, Energy 133 (Aug. 2017) 636–651.

[16] Y. Feng, et al., Operation characteristic and performance comparison of organic Rankine cycle (ORC) for low-grade waste heat using R245fa, R123 and their mixtures, Energy Convers. Manag. 144 (Jul. 2017) 153–163.

[17] L. Li, Y.T. Ge, X. Luo, S.A. Tassou, Experimental investigations into power generation with low grade waste heat and R245fa Organic Rankine Cycles (ORCs), Appl. Therm. Eng. 115 (Mar. 2017) 815–824.

[18] M. Ashouri, F. Razi Astaraei, R. Ghasempour, M.H. Ahmadi, M. Feidt, Thermodynamic and economic evaluation of a small-scale organic Rankine cycle integrated with a concentrating solar collector, Int. J. Low Carbon Technol. (August 2015) (2015) ctv025.

[19] D. Tiwari, A.F. Sherwani, N. Kumar, "Optimization and thermo-economic performance analysis of organic Rankine cycles using mixture working fluids driven by solar energy," *Energy Sources*, Part A Recover. Util. Environ. Eff. 41 (15) (2019) 1890–1907.

[20] R. Chacartegui, L. Vigna, J.A. Becerra, V. Verda, Analysis of two heat storage integrations for an Organic Rankine Cycle Parabolic trough solar power plant, Energy Convers. Manag. 125 (2016) 353–367.

[21] D. Casartelli, M. Binotti, P. Silva, E. Macchi, E. Roccaro, T. Passera, Power block off-design control strategies for indirect solar ORC cycles, Energy Procedia 69 (2015) 1220–1230.

[22] G. Cau, D. Cocco, Comparison of medium-size concentrating solar power plants based on parabolic trough and linear Fresnel collectors, Energy Procedia 45 (2014) 101–110.

[23] F. Ferrara, A. Gimelli, A. Luongo, Small-scale concentrated solar power (CSP) plant: ORCs comparison for different organic fluids, Energy Procedia 45 (2014) 217–226.

[24] E. Bellos, C. Tzivanidis, Parametric analysis and optimization of a solar driven trigeneration system based on ORC and absorption heat pump, J. Clean. Prod. 161 (2017) 493–509.

[25] A. Baccioli, M. Antonelli, U. Desideri, Dynamic modeling of a solar ORC with compound parabolic collectors: annual production and comparison with steady-state simulation, Energy Convers. Manag. 148 (2017) 708–723.

[26] S. Sonsaree, T. Asaoka, S. Jiajitsawat, H. Aguirre, K. Tanaka, A small-scale solar Organic Rankine Cycle power plant in Thailand: three types of non-concentrating solar collectors, Sol. Energy 162 (September 2017) (2018) 541–560.

[27] Milad Ashouri, Mohammad H. Ahmadi, Michel Feidt, Fatemeh Razi Astaraei, Exergy and energy analysis of a regenerative organic Rankine cycle based on flat plate solar collectors, Mech. Ind. 18 (2) (2017) 217.

[28] A. Ramos, M.A. Chatzopoulou, J. Freeman, C.N. Markides, Optimisation of a high-efficiency solar-driven organic Rankine cycle for applications in the built environment, Appl. Energy 228 (July) (2018) 755–765.

[29] A. Arteconi, L. Del Zotto, R. Tascioni, L. Cioccolanti, Modelling system integration of a micro solar Organic Rankine Cycle plant into a residential building, Appl. Energy 251 (January) (2019) 113408.

[30] M. Vanegas, O. Churio, G. Valencia, E. Villicaña, A. Ospino, Cálculo de las radiaciones total, directa y difusa a través de la transmisibilidad atmosférica en los departamentos del Cesar, La Guajira y Magdalena (Colombia) Calculation of total, direct and difusse radiation, through the atmospheric transmissivity in, Rev. Espac. 38 (7) (2017) 3.

[31] G. Valencia Ochoa, C. Acevedo Peñaloza, J.P. Rojas, Thermoeconomic modelling and parametric study of a simple ORC for the recovery of waste heat in a 2 MW gas engine under different working fluids, Appl. Sci. 9 (2019) 21.

[32] L. Cioccolanti, S. Rajabi Hamedani, M. Villarini, Environmental and energy assessment of a small-scale solar Organic Rankine Cycle trigeneration system based on Compound Parabolic Collectors, Energy Convers. Manag. 198 (June) (2019) 111829.

[33] C. Liu, et al., The environmental impact of organic Rankine cycle for waste heat recovery through life-cycle assessment, Energy 56 (2013) 144–154.

[34] K. Hossin, K. Mahkamov, B. Belgasim, Thermodynamic analysis and sizing of a small scale solar thermal power system based on organic rankine cycle, J. Sustain. Dev. Energy Water Environ. Syst. (2020).

[35] E.D. Kerme, A. Chafidz, O.P. Agboola, J. Orfi, A.H. Fakeeha, A.S. Al-Fatesh, Energetic and exergetic analysis of solar-powered lithium bromide-water absorption cooling system, J. Clean. Prod. 151 (2017) 60–73.

[36] M. Stucki, N. Jungbluth, Update of the Life Cycle Inventories of Solar Collectors, Uster, 2010.

[37] D. Tiwari, A.F. Sherwani, D. Atheaya, A. Kumar, N. Kumar, Thermodynamic analysis of Organic Rankine cycle driven by reversed absorber hybrid photovoltaic thermal compound parabolic concentrator system, Renew. Energy 147 (Mar. 2020) 2118–2127.

[38] O.A. Oyewunmi, C.J.W. Kirmse, A.M. Pantaleo, C.N. Markides, Performance of working-fluid mixtures in ORC-CHP systems for different heat-demand segments and heat-recovery temperature levels, Energy Convers. Manag. 148 (2017) 1508–1524.

[39] J. Cardenas Gutierrez, G. Valencia Ochoa, J. Duarte-Forero, Regenerative organic rankine cycle as bottoming cycle of an industrial gas engine: traditional and advanced exergetic analysis, Appl. Sci. 10 (13) (Jun. 2020) 4411.

[40] K.J. Ptasinski, Efficiency of Biomass Energy: an Exergy Approach to Biofuels, Power, and Biorefineries, Wiley, 2016.

[41] E. Bellos, C. Tzivanidis, Parametric analysis and optimization of an Organic Rankine Cycle with nanofluid based solar parabolic trough collectors, Renew. Energy 114 (2017) 1376–1393.

[42] J. Lizana, C. Bordin, T. Rajabloo, Integration of solar latent heat storage towards optimal small-scale combined heat and power generation by Organic Rankine Cycle, J. Energy Storage 29 (2020) 101367.

[43] W.A. Beckman, Solar Engineering of Thermal Processes, John Wiley & Sons, Inc., Hoboken, New Jersey, 2013.

[44] M. Maeiss, Flat Plate Collectors as Facade Elements for Domestic Water Heating and thermal Insulation, 1982.

[45] B.K. Hodge, Alternative Energy Systems and Applications, John Wiley & Sons, Inc., 2017.

[46] G. Valencia Ochoa, J. Cárdenas Gutierrez, J. Duarte Forero, Exergy, economic, and life-cycle assessment of ORC system for waste heat recovery in a natural gas internal combustion engine, Resources 9 (1) (Jan. 2020) 2.

[47] G. Valencia Ochoa, J. Piero Rojas, J. Duarte Forero, Advance exergo-economic analysis of a waste heat recovery system using ORC for a bottoming natural gas engine, Energies 13 (1) (Jan. 2020) 267.

[48] T.J. Kotas, The Exergy Method of Thermal Plant Analysis, Butterwort. Elsevier, 1985.

[49] R. Petela, Exergy analysis of the solar cylindrical-parabolic cooker, Sol. Energy 79 (3) (2005) 221–233.

[50] A. Bejan, G. Tsatsaronis, M.J. Moran, Thermal Design and Optimization, John Wiley & Sons, Inc., 1995.

[51] ISO, ISO 14000 Environmental Management Systems International Organization for Standardization, Switzerland, Geneva, CH, 2015.

[52] B. Thonon, Design method for plate evaporators and condensers, in: 1st International Conference on Process Intensification for the Chemical Industry, 1995, pp. 37–47.

[53] G.V. Ochoa, C. Isaza-Roldan, J.D. Forero, Economic and exergo-advance analysis of a waste heat recovery system based on regenerative organic Rankine cycle under organic fluids with low global warming potential, Energies 16 (3) (2020).

[54] M.G. Cooper, Saturation nucleate pool boiling - a simple correlation, in: Institution of Chemical Engineers Symposium Series, Jan. 1984, pp. 785–793, no. 86.

[55] G. Valencia, M. Vanegas, E. Villicaña, Disponibilidad geográfica y temporal de la Energía Solar en la Costa Caribe Colombiana, in: Sello Editor, 1, Univ. del Atlántico, 2016, pp. 17–28.

[56] J. Song, Y. Song, C. wei Gu, Thermodynamic analysis and performance optimization of an Organic Rankine Cycle (ORC) waste heat recovery system for marine diesel engines, Energy 82 (2015) 976–985.

[57] H. Tian, G. Shu, H. Wei, X. Liang, L. Liu, Fluids and parameters optimization for the organic Rankine cycles (ORCs) used in exhaust heat recovery of Internal Combustion Engine (ICE), Energy 47 (1) (2012) 125–136.

[58] W. Fan, Z. Han, P. Li, Y. Jia, Analysis of the thermodynamic performance of the organic Rankine cycle (ORC) based on the characteristic parameters of the working fluid and criterion for working fluid selection, Energy Convers. Manag. 211 (December 2019) (2020) 112746.